INDERSCIENCE PUBLISHERS
Linking academia, business and industry through research

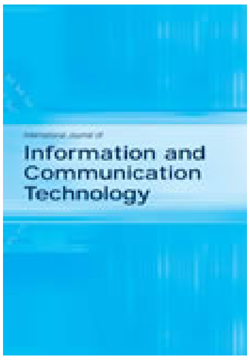

International Journal of Information and Communication Technology

ISSN online: 1741-8070 - ISSN print: 1466-6642
https://www.inderscience.com/ijict

Intelligent motor fault diagnosis based on deep learning

Yongchao Xie, Qing Chen, Jinyan Shi

Article History:

Received:	12 October 2024
Last revised:	02 January 2025
Accepted:	02 January 2025
Published online:	28 April 2025

Intelligent motor fault diagnosis based on deep learning

Yongchao Xie, Qing Chen* and Jinyan Shi

Hunan Railway Professional Technology College,
ZhuZhou, 412001, China
Email: xieyongchao2008@126.com
Email: hntdchenqing1980@126.com
Email: shijinyan2008@126.com
*Corresponding author

Abstract: In order to improve the effect of intelligent motor fault diagnosis, this paper proposes a motor fault diagnosis method based on deep transfer learning. The parameter identification module and deep neural network were used to solve the problem of accuracy reduction or non-identification of motor fault diagnosis methods based on deep learning neural network caused by motor dynamic parameters such as motor parameter drift and motor aging encountered in actual engineering. According to the experimental results, to a certain extent, it can solve the problem of neural network fault recognition accuracy decline caused by the problem of variable parameters of traditional neural network motor. It can be seen that the method proposed in this paper has certain effects, provides a large amount of engineering measured data for the problem of insufficient samples faced by complex machinery such as motors, and lays a good foundation for subsequent research.

Keywords: deep learning; motor; failure; intelligent diagnosis.

Reference to this paper should be made as follows: Xie, Y., Chen, Q. and Shi, J. (2025) 'Intelligent motor fault diagnosis based on deep learning', *Int. J. Information and Communication Technology*, Vol. 26, No. 9, pp.23–42.

Biographical notes: Yongchao Xie received his BSc in Communication Engineering from Lanzhou Jiaotong University, China and MSc in Communication and Information System from Southwest Jiaotong University, China. Currently, he is a Professor at the Hunan Railway Professional Technical College, and he is a key young teacher in Hunan Province, China. His research field is in centres on motor control technology.

Qing Chen received his BSc in Automation major from Tianjin University of Technology and Education, China and MSc in Software Engineering from East China Normal University, China. Currently, he is an Associate Professor at the Hunan Railway Professional Technical College, China. His research field is in centres on motor control technology and automation technology.

Jinyan Shi received her BSc in Machine Design and Automation from Lanzhou Jiaotong University, China and MSc in Drive Technology and Intelligent System from Southwest Jiaotong University, China. Currently, she is a Professor at the Hunan Railway Professional Technical College. Her research field is in centres on mechanical and electronic engineering.

1 Introduction

In recent years, with the improvement of scientific and technological level, motors have been widely used in coal, metallurgy, petroleum, chemical and other industrial fields, and are indispensable mechanical devices in modern industrial production. As an important power equipment in the industrial field, the stability and safety of motor operation have a direct impact on the safe and stable operation of various mechanical equipment. With the progress of motor manufacturing technology, there are many kinds of modern motors, and they are increasingly developing in the direction of high precision, automation and intelligence (Almounajjed et al., 2022).

In industrial production, the working conditions of motors are relatively complicated. Due to long-term high-load operation, high-intensity operation, foreign particles entering the motor, parts wear and tear, and untimely daily maintenance, it often leaves potential safety hazards for the stable operation of motors. Once the motor fails, it will not only affect the smooth operation of the equipment, but also cause certain economic losses to the enterprise, and even threaten the personal safety of on-site workers (AlShorman et al., 2020). As one of the important technologies in the field of fault diagnosis, intelligent diagnosis technology is an important means to realise the stable operation and efficient work of equipment. Therefore, in order to ensure the safe and stable operation of the motor and prevent major accidents, it is of great practical significance to study intelligent diagnosis methods for motor diagnosis (Cheng et al., 2021). Traditional signal processing methods usually collect signals reflecting the running state of the motor, extract the features containing fault information in the signals, and diagnose them through pattern recognition. This process often requires relevant personnel to have rich professional knowledge and experience in fault diagnosis, but for some signals with a lot of interference noise and insignificant fault information, specific diagnosis methods are needed and the effect is not good, and the diagnosis process is often affected by external environmental factors and its own factors (Gundewar and Kane, 2021).

With the development of computer technology, intelligent diagnosis technology based on machine learning has promoted the development of intelligent diagnosis field. As one of the hottest fields in machine learning, deep learning is widely used in machine translation, natural language processing, speech recognition, image recognition and other fields. Deep learning simulates the human brain's multi-layer analysis and learning ability, establishes a multi-layer perceptual neural network, directly analyses and judges the target, automatically extracts the features contained in the information, avoids information loss caused by human factors, simplifies the diagnosis process, and greatly improves the accuracy of fault diagnosis. Therefore, as one of the popular technologies in the field of intelligent diagnosis, deep learning has promoted the intelligent development of diagnostic technology.

In order to improve the effect of intelligent motor fault diagnosis, this paper proposes a motor fault diagnosis method based on deep transfer learning, and uses the parameter identification module (PIM) and deep neural network to solve the problem of accuracy reduction or non-identification of motor fault diagnosis methods based on deep learning neural network caused by motor dynamic parameters such as motor parameter drift and motor aging encountered in actual engineering. In addition, in order to make full use of the advantages of vibration and current signals in motor fault diagnosis, this paper proposes a knowledge transfer method between modes.

The main innovation of this method is to explicitly add the characteristics of motor parameter change information to the classifier network by embedding the PIM in the neural network model. By combining the domain adaptive method and small sample learning method, the ability of resisting variable parameters and the performance of small sample learning in fault diagnosis are improved.

A cross modal knowledge transfer method from vibration signal model to current signal model is designed. Through the design of feature alignment between different modal models and knowledge distillation in the output layer, the fault diagnosis knowledge learned from the vibration signal model is transferred to the current signal model to achieve better fault diagnosis performance without relying on the vibration signal in the reasoning stage. The effectiveness of the proposed method is verified on the multi-modal fault dataset of electric UAV motor.

2 Related works

Motor signal acquisition is the premise of motor fault diagnosis, and it mainly collects and analyses temperature, vibration, current and other signals. Motor temperature signal acquisition mainly places temperature sensors at sensitive parts such as bearing ends and stators in advance to collect the temperature of each part of the motor for diagnosis and analysis. Lang et al. (2021) introduced the change and measurement of rotor temperature when the motor fails. Vibration signal acquisition is mainly aimed at whether the motor has mechanical faults. Usually, acceleration sensors are selected and pre-installed in bearings, fans, bases and other parts where mechanical faults may occur. Because the motor often produces abnormal vibration when it fails, the vibration signal usually contains a large number of fault characteristics of motor operation. Therefore, the type and location of the fault can be judged by analysing the characteristic values such as frequency and amplitude of the vibration signal. In Liang et al. (2021), the envelope signal containing fault characteristic information was obtained by spectral kurtosis method and Hilben envelope demodulation, which highlighted the fault characteristic information and quickly and effectively identifies the characteristic frequency of the fault signal. Current signal acquisition is mainly aimed at whether the motor has an electrical fault. Because the fault will cause the change of stator current, a current sensor is usually installed in advance to collect the motor stator current signal. Lin (2021a) made fuzzy diagnosis of motor inter-turn short circuit fault by collecting current signal. The diagnosis results show that this method can well reflect the degree of motor inter-turn fault. Lin (2021b) used discrete wavelet transform algorithm to extract the fault characteristics of current signals, and effectively identified the characteristic frequency of fault signals.

Fourier transform (FT) can transform the signal in the time domain to the corresponding frequency domain, and the abnormal state of the signal can be more intuitively identified according to the frequency domain. However, the FT is completely transformed in the frequency domain. Because of the transformation of the integral function, the unstationary part of the signal becomes smooth, and it is easy to lose the useful information contained in the original signal without time domain information. Therefore, most FTs are aimed at linear stationary signals (Long et al., 2021a). Short-time Fourier is an improvement of FT, and it uses nonlinear stationary signals as the superposition of short-time linear stationary signals, and is achieved by windowing the time domain window, and translating this window can cover the whole time domain. In this way, the time-frequency representation of the signal can be obtained by FT transforming the signal in each window (Long et al., 2021b). Nath et al. (2021) processed the fault signal by windowed interpolation fast FT. Niu et al. (2023) used the nonlinear short-time Fourier transform (NLSTFT) method to accurately estimate the instantaneous frequency of vibration signals. The decisive factor of short-time Fourier transform (STFT) is the window function, which is essentially based on single resolution analysis. Therefore, if the resolution needs to be changed, the corresponding window function must be re-selected.

There are many deep learning models, which are mostly used in the fields of speech and image recognition, computer vision, information retrieval and fault diagnosis. Wen Jiangtao et al. combined compressed sensing theory with deep learning. In order to reduce the redundant information of data without losing useful information, compressed sensing theory was introduced to process data. Finally, deep learning was used to diagnose faults and obtain high accuracy (Saha et al., 2022). Shao et al. (2020) used deep network to extract the joint features after spectrum and time domain fusion, and used particle swarm support vector machine to diagnose the joint features, which improved the diagnosis accuracy and verifies the adaptability of deep learning. Shen et al. (2020) introduced deep learning models into fault diagnosis. Through simulation experiments, it shows that deep learning has certain advantages in improving diagnosis accuracy and is feasible in this field.

The signals collected in the motor are usually one-dimensional time domain signals. In order to use a two-dimensional convolutional neural network for feature extraction, the collected signals need to be converted into two-dimensional grid data. At the same time, the relationship between each data point and its upper, lower, left and right data points contains useful information. Because the motor fault signal is usually non-stationary, its characteristics change with time and working conditions. However, because the motor rotation is periodical, it can be considered that it has the characteristics of short-term stability (Sun et al., 2022).

STFT can increase the characteristic reflection of FT in time dimension by windowing the input signal in FT. For one-dimensional signal, its output is a two-dimensional matrix of time and spectrum, which is a means to extract the characteristics of non-stationary signals. Compared with wavelet transform, it is more efficient for grid output processing data (Tang et al., 2020).

3 Network structure design and training of fault diagnosis methods

3.1 Signal pre-processing

Considering the grid characteristics of the input signal of the feature extraction neural network, the size of GPU memory and the computational efficiency, the data with a sampling time $T(s)$ of one second is selected as a data input, and the output matrix size is 256×256. Therefore, if the sampling frequency is f_s (Hz), the number of data is $T \times f_s$. Hamming window is selected as the window function, the selection of overlap rate shall be determined according to the characteristics of the signal. If the signal contains important high-frequency components, a high overlap rate can help retain this information. However, the motor signal processed in this paper is mainly high-frequency components, and selecting a higher overlap rate can effectively improve the accuracy of data processing High overlap rate will bring high load pressure to the system. Considering the hardware conditions of the system in this paper, the window overlap ratio is α = 0.8, and the window length W is calculated according to the following formula (Wang and Xu, 2021):

$$wide = \frac{T \times f_s - (W - \alpha \times W)}{W - \alpha \times W} \tag{1}$$

Among them, α = 0.8. The output matrix frequency range is selected according to the relationship between the motor speed range and the fault frequency, and the STFT algorithm is used to convert the input timing sequence signal into a two-dimensional matrix. The dataset used in this paper uses CWRU motor bearing fault dataset and MFPT motor bearing fault dataset. Frequency selection is based on the combination of these two datasets. The frequency range selected in this paper is 0~6,000 Hz. This frequency is also one of the basic parameters of the subsequent experimental study in this paper. Figure 1 shows the 0.2 second motor bearing fault acceleration signal and the two-dimensional matrix diagram obtained by STFT of the signal data.

Figure 1 Process of signal conversion into two-dimensional matrix (see online version for colours)

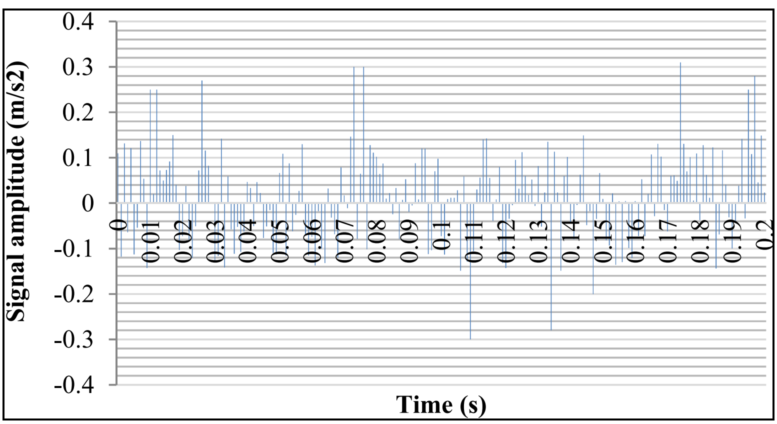

3.2 Network structure

The dense module is the core of DenseNet, which represents how data is connected and propagated between convolutional modules in the network, and consists of multiple convolutional modules. The convolution module includes a convolution layer, an activation function and a batch normalisation layer. Its characteristic is that the input and output matrices are the same size. The purpose is to facilitate the splicing of the convolution module output in the dense module in the channel dimension. The connections inside the dense module are shown in Figure 2. The number of output channels of each convolutional layer is also called the growth rate of the dense module. Moreover, all convolutional layers in the same dense module have the same output dimension and the same output matrix size. The output of each layer will be connected to the input of all subsequent convolutional layers. splicing, so the number of output channels in each layer can be expressed as (Wang et al., 2020):

$$OC_n = IC + (N + 1 - N) \times OC \quad (2)$$

Among them, OC_n represents the number of output channels of the convolutional module of the n^{th} layer, IC and OC respectively represent the number of input channels and the number of output channels of a single convolutional layer, and OC is also equal to the number of convolution kernels in the convolutional layer, and N represents the number of convolution modules contained in the dense module. The network and parameter capacity can be adjusted by adjusting the number and growth rate of convolution modules in dense modules.

Figure 2 Dense module (see online version for colours)

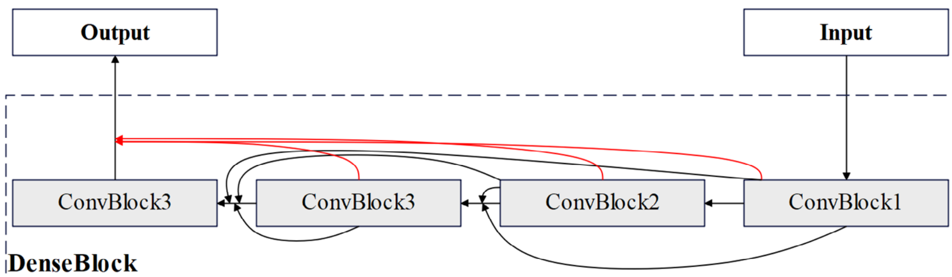

In this paper, the neural network structure is used for parameter identification (Figure 3). The structure of the module, predicted parameters, etc. can be customised according to the needs. When the output is a continuous variable, it is necessary to specify the parameter variation range in advance, so as to improve the resolution of neural network parameter recognition and facilitate label normalisation. The number of prediction parameters is the number of neurons output by the module.

Considering the GPU capacity and training data size, the structural design of the four-class discriminant classifier in this paper is shown in Figure 4(a). Among them, the function of the ID-flatten layer is to convert the three-dimensional tensor obtained from the feature extractor into a one-dimensional vector that can be used by the densely connected layer (Xue et al., 2022).

Figure 3 Network structure of single PIM

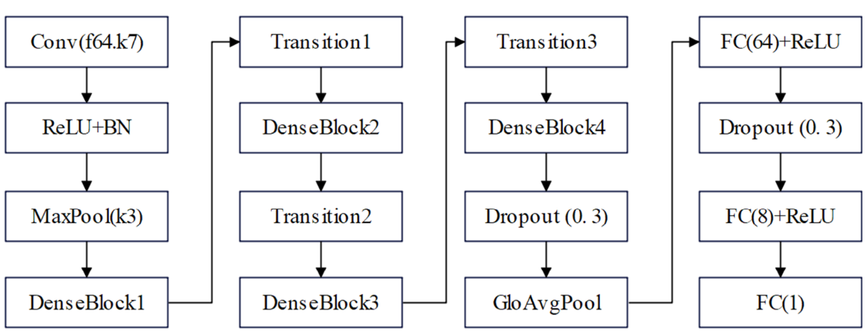

Figure 4 Classifier network, (a) discriminative classifier (b) measurement based small sample classifier

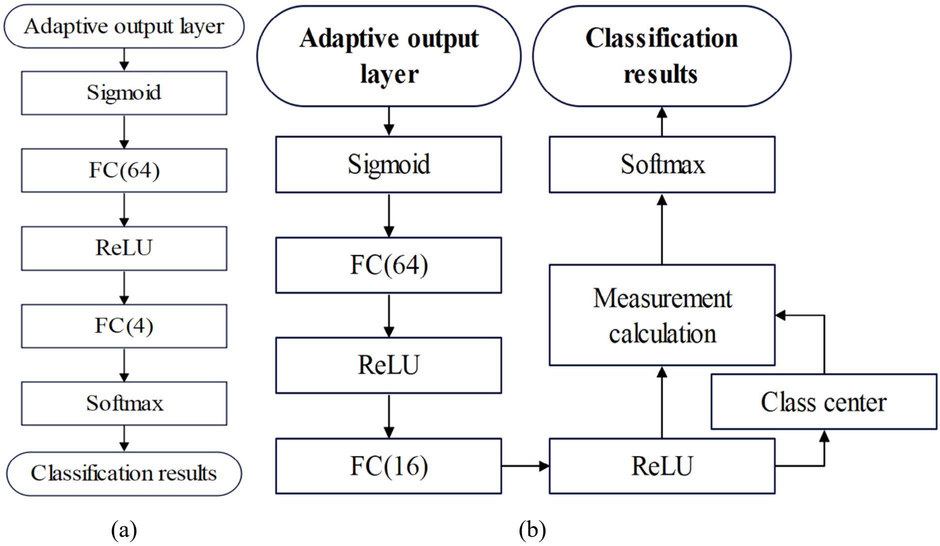

The structure of the small sample classifier is shown in Figure 4(b). Different from the discriminant classifier, which directly outputs the classification results from the fully connected network, this small sample classifier uses the feature calculation of the Support set data to obtain the class centre, and uses the distance measure of the test sample from the class centre in the feature space as the output, and then outputs the classification probability prediction in the form of Softmax layer one-hot.

3.3 Network domain adaptive architecture

Domain adaptive learning of feature edge distribution in the network can help the network further improve the stability of network performance under various parameters. Borrowing source domain data as prior knowledge, only a small amount of target domain data is used to build a high-performance target domain deep network model, which enables the network to maintain high accuracy when used in motors under new unknown parameters. In this paper, discriminant network method is used for domain adaptive learning. Its structure is shown in Figure 5(a). The adaptive layer network structure is shown in Figure 5(c) (Yin and Cen, 2022).

The domain discriminator is similar to the classifier network for discriminating whether features in the adaptive layer originate from the source domain or the target domain. When the domain discriminator is trained, the parameters are fixed, and the data of the source domain and the target domain are randomly passed into the data of the source domain and the target domain, and the adaptive network layer is trained by controlling the loss function to ensure that the classifier keeps high accuracy, so that the output features of the adaptive layer are approximate when the input of the source domain and the input of the target domain, thus reducing the recognition accuracy of the domain discriminator and making the edge distribution of the network features approximate.

Combining the network structure of feature extractor and classifier, this paper designs a domain discriminator as shown in Figure 5(b) (Zhang et al., 2022).

Figure 5 Domain adaptive network structure, (a) overall network connection diagram (b) domain classifier network structure (c) adaptive layer network

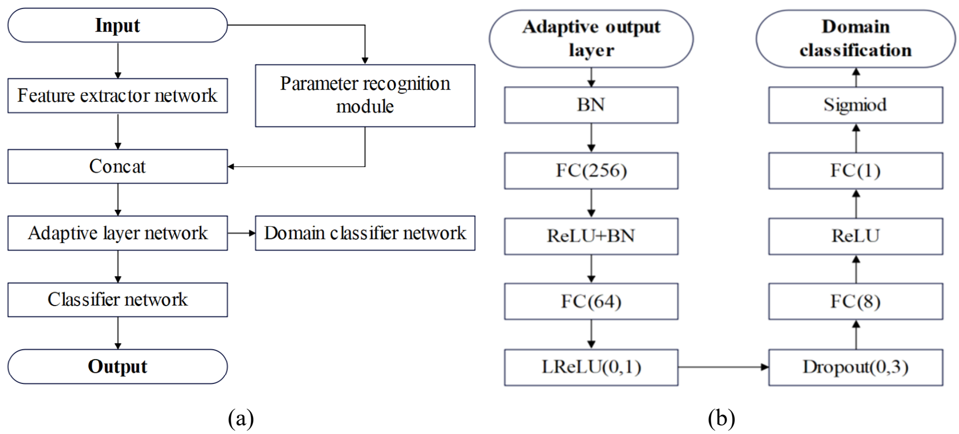

3.4 *Model training and fault diagnosis methods*

The network training method in this paper is:

1 Training parameter recognition network: According to the principle of motor, the prediction parameters and parameter range are selected, and the training dataset with the prediction parameters as labels is constructed, and the parameter identification network structure is constructed. If the predicted parameters are continuous values, the parameters are normalised according to the parameter range as training labels.

2 Training the feature extraction network: The feature extraction network structure is built, and the probabilistic discriminant classifier structure is built. Then, the gray image obtained from the motor signal is taken as the input, the fault classification is taken as the output dataset, the Cross-Entropy is taken as the loss function, and the Adam is taken as the optimisation algorithm. The feature extractor inputs the gray image, outputs the input of the connection classifier and the actual value of the network prediction parameter is connected to the input of the classifier, and its structure is shown in Figure 6.

3 Training domain classifier: The domain classifier with domain adaptive structure is constructed, and the target domain and source domain data are randomly mixed in a ratio of 1: 1 to construct a dataset. If there is too little data in the target domain, the ratio of source domain data can be appropriately increased to 1.3: 1. Then, the source domain data label is added as 0, the target domain data label is 1, and binary-cross-entropy is taken as the loss function. The feature extraction network, the adaptive layer and the domain classifier network are connected in series, and the domain classifier is trained to make its discrimination accuracy reach about 80%.

4 Training the adaptive layer: The feature extractor, the adaptive layer and the classifier are connected, and the domain classifier is connected after the adaptive layer. According to the requirements, the PIM can be connected, and its structure is shown in Figure 7. The classifier loss function ℓ_c (D_s, γ_s) and the domain classifier loss function ℓ_{domain} (D_s, γ_s) are constructed, and the sum of the two loss functions is taken as the overall loss function ℓ_{total}, which can be expressed as:

$$\ell_{total} = \ell_c\left(D_s, \gamma_s\right) + \lambda \ell_{domain}\left(D_s, \gamma_t\right) \tag{3}$$

Among them, λ is the weight coefficient, which takes different values according to the difference of loss function and network output structure. The degree to which the source domain sample classification accuracy limits the domain adaptive layer transformation can be adjusted by the adjusted value of λ, and engineering experience is ℓ_c:$\lambda\ell_{domain} \approx 2$:1.

Figure 6 Training structure diagram of feature extraction network

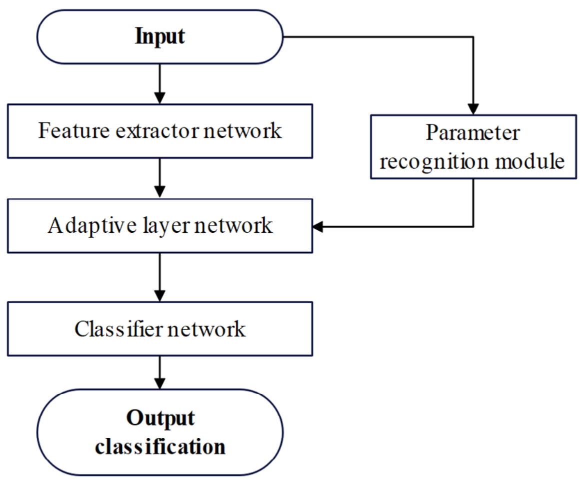

5 The algorithm repeats steps 3 and step 4, and increases the discrimination accuracy in step 3 to 70 ~ 80% each time, until the domain discrimination accuracy in step 4 decreases to 50%, and the overall loss no longer decreases.

6 When there is very little data in the target domain, the probabilistic discriminant classifier based on cross entropy after migration may not be able to distinguish features, so it is necessary to build a small sample learning classifier model to improve network performance. The trained network classifier structure in step 5 is replaced with the small sample classifier in Figure 5(b), the weight of FC (64) layer is initialised to the weight of FC (64) of the discriminant classifier in Figure 5(a), and the trained feature extraction network, adaptive layer and PIM are connected. The labelled data of the source domain is used to form the support set in the form of N-way K-shot, and the data of the target domain is used to form the query set, and the Euclidean distance is selected as the spatial metric function $d(\cdot)$. First, the central point of each class in the Support set is calculated, and the calculation formula is:

$$c_n = \sum_{(x_i, y_i)} \frac{x_i}{k} \tag{4}$$

c_n is the centre point coordinate of the n^{th} class in the N class, S_n represents all samples belonging to the n^{th} class in the support set, and k is the number of samples of each class in the support set.

Figure 7 Adaptive layer training

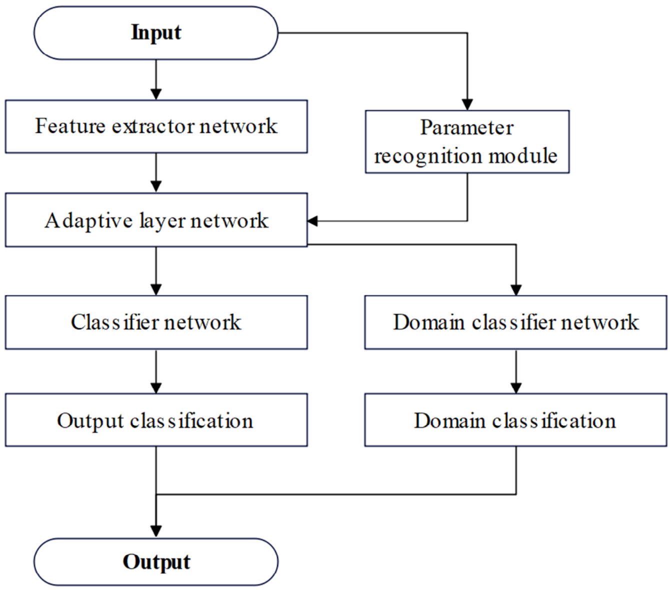

Then, the algorithm calculates the distance between c_n and Q_n through the spatial metric function, and Q_n represents all samples belonging to the n^{th} class in the query set. The resulting distance is calculated by the softmax layer as the probability:

$$P_i(n) = \frac{\exp\left(-d\left(g_f(x_i), c_n\right)\right)}{\sum_n^N \exp\left(-d\left(g_f(x_i), c_n\right)\right)} \tag{5}$$

$P_i(n)$ represents the probability that the sample x_i of the query set is in the n^{th} class, and $g_f(\cdot)$ is the mapping function between the sample and the feature space. Therefore, the metric loss function l_d is defined as:

$$l_d = -\sum_{(x_i, y_i) \in Q_n} \sum_n^N y_i \log\left(P_i(n)\right) \tag{6}$$

When the sample in Q_n has no label, y_i is the category of u closest to the sample. Setting the small sample classifier parameters can train all parameters of other layers of the fixed network. Using Adam as the optimiser to train the classifier network until the verification set loss function is minimised, the centre point coordinates of the current Epoch are saved as a local file after each training.

The calculation method of smoothing formula layer in this paper is as follows:

$$\hat{\alpha}_i = \alpha_i + \frac{\lambda}{N}\sum_{i=1}^{N}\alpha_i \tag{7}$$

Among them, $\hat{\alpha}_i$ is the prediction parameter of the actual output of the current input grey image, α_i is the output parameter of the PIM of the previous input grey image, $\sum_{i=1}^{N}\alpha_i/N$ represents the average value of the output parameter of the identification module of the previous input grey image from the current time to the previous *N*, and *λ* is the weight coefficient used to adjust the stability degree.

When the small sample classifier is used for fault diagnosis, the dotted line part of the small sample classifier in Figure 5(b) is not connected, and the class centre coordinates are directly obtained by reading the local file saved during training.

3.5 Research on knowledge transfer between modes of vibration signal model and current signal model

The analysis of this paper is based on the following three assumptions:

1. The bearing is a rigid body without significant deformation.
2. The outer ring is fixed.
3. There is no sliding friction in the rolling elements.

As shown in Table 1, the theoretical vibration frequencies of faults in different parts can be obtained. In the table, *d* represents the diameter of rolling elements, *D* represents the pitch circle diameter of rolling elements, *f* represents the inner ring rotation speed, *α* represents the contact angle, and *n* represents the number of rolling elements.

Table 1 Theoretical frequency of different bearing failures

Fault location	*Vibration frequency*
Outer ring failure	$\frac{nf}{2}\left(1-\frac{d}{D}\cos\alpha\right)$
Inner ring failure	$\frac{nf}{2}\left(1+\frac{d}{D}\cos\alpha\right)$
Cage failure	$\frac{f}{2}\left(1-\frac{d}{D}\cos\alpha\right)$
Rolling element failure	$\frac{Df}{2d}\left(1-\left(\frac{d}{D}\cos\alpha\right)^2\right)$

When a single point of failure occurs in the motor bearing, its load torque changes, so the load torque of the motor can be expressed by formula (8):

$$T_L = T_{L0} + \vartriangle T \sum_{k=-\infty}^{+\infty} \delta\left(t - \frac{k}{f_c}\right) \tag{8}$$

In the formula, T_{L0} represents the constant component of torque, $\delta\left(t - \frac{k}{f_c}\right)$ represents the torque excited by bearing fault, f_c represents the characteristic frequency of bearing failure. Furthermore, according to the kinematics equation, formula (9) can be obtained.

$$\omega = \omega_0 + \vartriangle\omega \sum_{k=-\infty}^{+\infty} \delta\left(t - \frac{k}{f_c}\right) \tag{9}$$

In the formula, ω_0 represents the constant component of the rotational speed, and $\sum_{k=-\infty}^{+\infty} \delta\left(t - \frac{k}{f_c}\right)$ is the fluctuation component of the rotational speed. According to the speed formula of the motor, the back electromotive force of the motor can be obtained, as shown in formula (10).

$$e = e_0 \sin\left(P \cdot 2\pi f_r t\right) + \vartriangle e \sin\left(P \cdot 2\pi f_r t\right) \cdot \sum_{k=0}^{+\infty} \delta\left(t - \frac{k}{f_c}\right) \tag{10}$$

According to the current principle, the input current expression of the motor stator can be further obtained, as shown in formula (11).

$$I = \frac{U - e}{R + j \cdot P\omega_r L} = \sum_{k=1}^{\infty} I_k \sin\left(2\pi Pk \cdot f_r t + \varphi_0\right) + \vartriangle I_k \sin\left(2\pi\left(P \cdot f_r \pm kf_c\right)t + \varphi_k\right) \tag{11}$$

From the above analysis, it can be obtained that the current signal of the motor contains the characteristic frequency $P \cdot f_r \pm kf_c$ of motor bearing fault, and in the formula, f_r represents the frequency of the power supply and f_c represents the characteristic frequency of bearing fault.

In order to amplify the generalisation information contained in the 'soft label' of the original modal model, the temperature parameter T is introduced to heat up the knowledge of the 'soft label'. The calculation formula is shown in formula (12).

$$q_i = \frac{\exp\left(z_i / T\right)}{\sum_j \exp\left(z_i / T\right)} \tag{12}$$

In the formula, z_i represents the predicted value of the i^{th} category in the model output, q_i is the soft label after temperature increase, and T represents the temperature (when $T = 1$, it degenerates to the standard softmax function). In the training process, the KL divergence of the soft label after heating by formula (12) is obtained by minimising the target modal model and the original modal model classifier [as shown in formula (13)], so that the target modal model can learn the knowledge of the original modal model.

$$D_{KL}\left(p\|q\right)=H(p,q)-H(p)=-\sum_{x}p(x)\log q(x)-\sum_{x}-p(x)\log q(x)$$
$$=-\sum_{x}p(x)\left(\log q(x)-\log p(x)\right)=-\sum_{x}p(x)\log\frac{q(x)}{p(x)} \tag{13}$$

At the same time, by minimising the mean square error (MSE) of the output feature vectors of the target modal model and the original modal model feature layer, the target modal model can further learn the feature extraction knowledge of the original modal model through the intermediate feature layer. The objective function of inter-modal knowledge transfer learning can be written as formula (14):

$$L=L_c+\alpha L_{distance}+\beta L_{distill} \tag{14}$$

In the formula, L is the total loss function of model training, L_c represents the supervised learning loss, $L_{distance}$ represents the distance loss of the mean square error of the feature layer between the target modal model and the original modal model, $L_{distill}$ represents the KL divergence loss of the classifier output between the target modal model and the original modal model, and α and β represent the knowledge transfer loss weight.

4 Experimental studies

4.1 Experimental environment

The experimental platform of this paper is set as i9 processor, GPU is GTX1080, video memory is 16G, operating system is Windows 10, deep learning framework is PyTorch 1.7, IDE is Jupyter Notebook, data pre-processing uses MATLAB 2022, Python version is 3.7, Cuda version is 10.1.

The network experimental dataset uses the motor bearing fault dataset of CWRU versus the MFPT motor bearing fault dataset.

The pre-processing parameters are set to have a sampling time of 1 second, an overlap rate of 50%, an output grey pixel of 256 * 256 ×, and a frequency range of 0~6 kHz. After pre-processing the dataset, 7,005 CWRU datasets are obtained, including 551 normal data, 1,708 inner ring fault data, 2,999 outer ring fault data and 1,747 roller fault data. After pre-processing the MFPT dataset, 32 pieces of normal data, 36 pieces of inner ring fault variable load data, 32 pieces of outer ring fault constant load data and 36 pieces of variable load data are obtained.

The motor surface vibration acceleration signal is used as the characteristic fault signal input, and the load is used as a single variable parameter in all experiments to identify the bearing fault of the motor. The CWRU dataset is divided into four types of datasets: A, B, C and D according to four loads of 0, 1, 2 and 3. Moreover, each class of dataset contains all types of fault signals. In addition, a dataset composed of a variety of load data is also combined. For example, class A, B, and C data are combined with the fault type as the combination dimension as class A/B/C source domain data, and the target domain datasettings are also combined in this way. The merged dataset precision and F1 are shown by the classification results according to the sum of all classes contained in the dataset.

In this experiment, CWRU dataset is used to measure the basic performance of speed network with four kinds of datasets: A, B, C and D divided by load as type variable. The changes of network fault diagnosis accuracy when load changes are compared, and the changes of network accuracy when PIM is used and not used are compared.

Accuracy (*Acc*) is one of the main indicators for judging classification performance, defined as the proportion of correctly classified samples to the total number of test samples. Its calculation is:

$$Acc = \frac{TP}{TP + TN + FP + FN} \tag{15}$$

The parameter explanation is as follows: *TP*: true positive, *FN*: false negative, *FP*: false positive, and *TN*: true negative.

Using the top 50% of the raw data for each fault category, obtain 2,000 training samples for each category under each speed condition. The remaining 50% of the raw data is sampled non overlapping, generating 500 test samples for each category at each speed to obtain the test domain data In order to verify the performance of the proposed method under limited training samples, a series of experiments were conducted by randomly selecting different numbers of training samples from the original training set to compare the performance of the model under different training sample conditions. The number of samples for each category in the series training set is 20, 40, 50, 100, 160, 400, 500, 1,000, 1,500, and 2,000 respectively. In order to eliminate the fluctuation of experimental results caused by random sampling, the experiment was repeated five times for each sample size to obtain the average test accuracy. The initial learning rate for model training is set to 0.0001.

4.2 Results

In order to fit the parameter changes, the parameter recognition module is first trained. The dataset is divided into the training set and the test set according to 7:3, epoch is 100, batch is 30, and the learning rate is 0.001. The average error of the test set is shown in Figure 8.

The training feature extractor, adaptive layer, classifier network is constructed, which is a batch size of 50. Moreover, 200 epoches are uniformly trained for each type of network, the learning rate is 0.001, the partition ratio of the dataset to the test set is 7: 3, and each Epoch in a single data domain takes about 11.2 seconds. The changes of accuracy rate and F1 during the training process that the training domain is A, the test domain is A, and PIM is not used and PIM is used, are drawn separately, as shown in Figure 9.The results of each experiment are recorded as the evaluation of the model parameters of the Epoch with the highest test set F1 among the 20 epoches before the end of training. Moreover, each experiment is repeated three times, and the average value of the three evaluations is taken to record the table. When the non-training domain is used for testing, all the data of the target domain are used for testing. The overall experimental results are shown in Table 2.

Table 3 further compares the recall rate results of different backbone networks using the knowledge transfer method between modes. S1–S9 respectively corresponds to nine motor health states: normal, bearing outer ring fault, bearing cage fault, bearing rolling element fault, bearing inner ring fault, rotor shaft bending, rotor permanent magnet demagnetisation, stator winding inter phase short circuit, and stator winding inter turn short circuit.

Figure 8 Training process of PIM (see online version for colours)

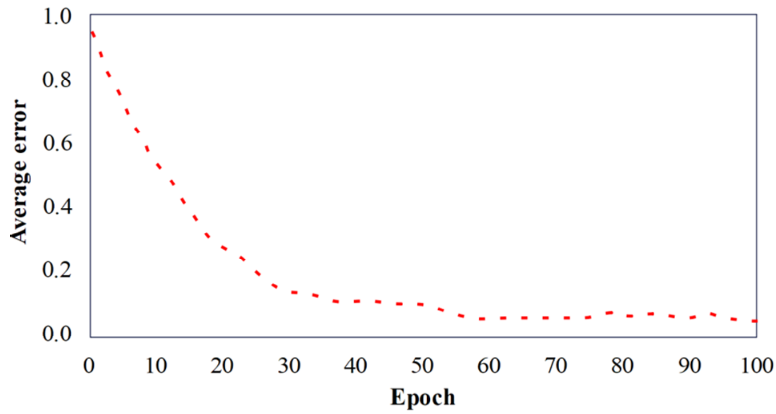

Table 2 Performance test results of variable load network (Acc: %)

Training domain	*Test domain*							
	A		*B*		*C*		*D*	
	Acc	*F1*	*Acc*	*F1*	*Acc*	*F1*	*Acc*	*F1*
A	97.42	0.98	67.12	0.65	66.23	0.64	48.02	0.35
A (+PIM)	97.61	0.98	70.29	0.68	64.75	0.61	51.98	0.40
B	72.86	0.75	98.60	0.99	90.39	0.91	67.32	0.70
B (+PIM)	70.29	0.73	98.51	0.99	90.19	0.92	63.95	0.66
C	70.59	0.73	91.38	0.92	98.41	0.98	72.96	0.74
C (+PIM)	64.94	0.72	90.59	0.92	98.70	0.99	85.64	0.85
D	54.85	0.44	74.84	0.75	82.37	0.85	96.53	0.97
D (+PIM)	60.98	0.67	81.58	0.86	93.65	0.95	99.00	0.99
A/B/C	95.63	0.97	97.42	0.98	97.71	0.98	87.12	0.87
A/B/C (+PIM)	97.81	0.98	98.70	0.99	98.90	0.99	88.90	0.91

Table 3 Comparison of recall rate (%) before and after knowledge transfer between modes

	S1	*S2*	*S3*	*S4*	*S5*	*S6*	*S7*	*S8*	*S9*
WDCNN	84.15	52.36	100	80.97	73.76	100	100	100	100
SDCNN	72.59	47.40	100	71.92	84.51	100	100	100	100
SDCNNRRD	96.00	66.68	100	77.94	68.90	100	100	100	100
WDCNN + MKT	73.65	80.61	100	85.86	89.36	100	100	100	100
SDCNN + MKT	81.56	83.67	100	80.83	87.03	100	100	100	100
Model in this article	84.53	82.77	100	82.34	87.70	100	100	100	100

Figure 9 Training process and real-time test results of class A dataset, (a) comparison results of accuracy of motor fault diagnosis training set (b) comparison results of accuracy of motor fault diagnosis test set (c) comparison of F1 test results for motor fault diagnosis data (see online version for colours)

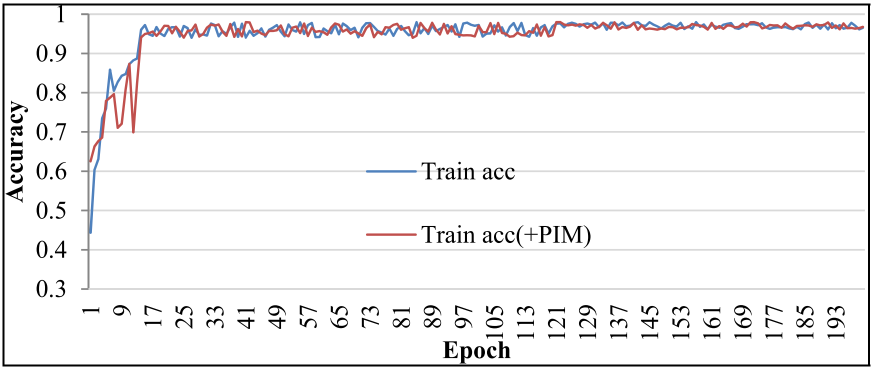

(a)

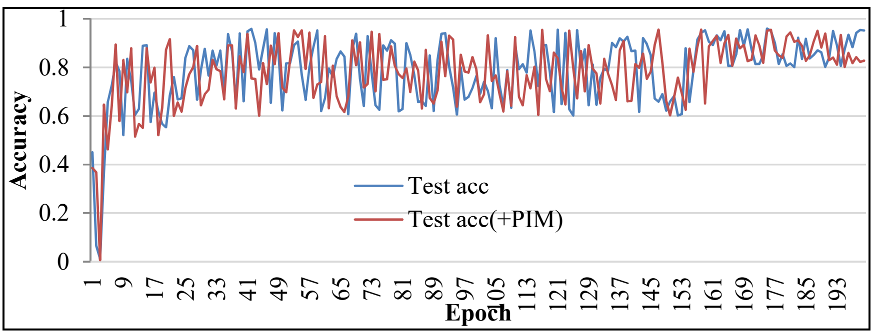

(b)

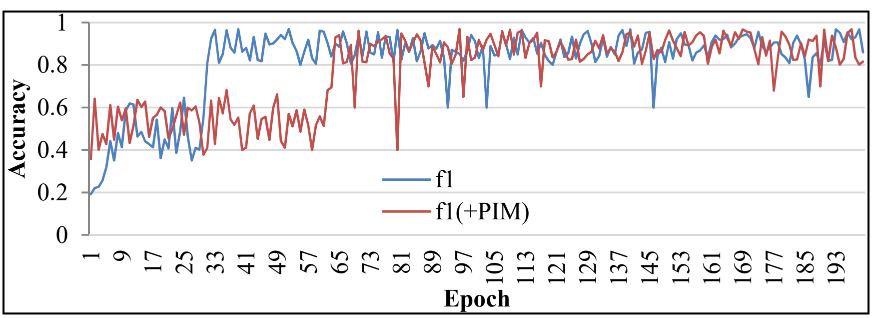

(c)

The average accuracy diagrams of non-source domains and non-source domains with PIM in each source domain are shown in Figure 10.

Figure 10 Histogram of accuracy results of performance test of variable load network (see online version for colours)

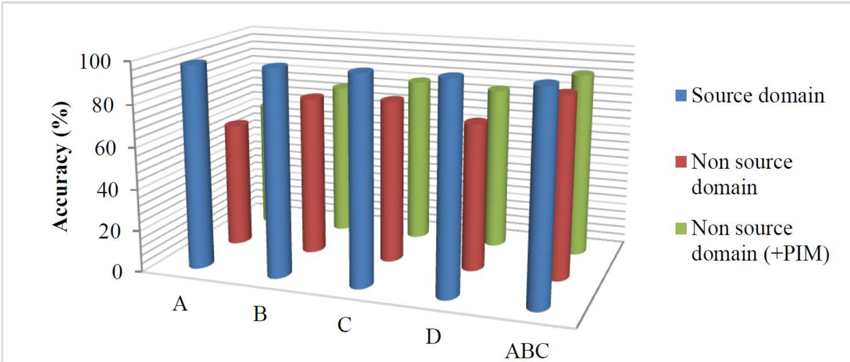

4.3 Analysis and discussion

It can be seen from Figure 8 that the average error between the predicted value and the true value of the parameter training parameter recognition module after 100 epoches is 0.05 (±0.1).

It can be found from Figure 9 that with the increase of network training times, the accuracy of the test set and F1 index gradually increase, and the network reaches an accuracy of about 96% and F1 of 0.95 at 60 epoches. In the two cases with and without PIM, the convergence curve and convergence speed of the network in the first 30 epoches are similar, but the network without PIM module converges faster during the improvement of accuracy from 93% to 97%. After that, the network accuracy can be stable at around 98% and no longer improve, and the frequency and range of accuracy fluctuations in subsequent Epoch gradually decrease. The main reason for the fluctuation of accuracy is that the number of categories in this experiment is small, and due to the limitation of hardware platform, the training method uses a smaller batch. When the randomly sampled batch deviates greatly from the overall data distribution or test set distribution, it is easy to make the model produce a large fluctuation of test accuracy, which can be alleviated by increasing the batch and reducing the learning rate.

It can be seen from Table 3 that the network feature extractor and classifier structure can achieve an accuracy of more than 97.5% for its own type of load data under 200 epoches. However, when the load parameters change, the accuracy of fault identification of the network changes greatly. From the test of class A network on classes B, C and D data, it can be seen that the load of B, C and D gradually increases compared with Class A network, and the parameter gap gradually becomes larger. Therefore, the recognition accuracy and feature distribution difference of Class A network on other data domains increase with the increase of load parameter gap. Therefore, it reflects that the change of motor load parameters can be correctly identified by the neural network in the dataset. When the training data is consistent with the test data, adding PIM improves 0.2%, –0.1%, 0.3% and 2.5% in the data domains A, B, C and D, respectively, compared with not adding PIM. Considering the model training error, it cannot be concluded that PIM has improved when the training data is consistent with the test data.

Careful observation of Table 3 shows that even without using the inter modal knowledge transfer method, the three backbone networks perform very well in four fault types: bearing cage fault, rotor shaft bending, rotor permanent magnet demagnetisation, stator winding inter phase short circuit and stator winding inter turn short circuit (S6–S9). However, the classification performance is weak in the four categories of normal, bearing outer ring fault, bearing rolling element fault and bearing inner ring fault. After applying the knowledge transfer method between modes proposed in this paper, the performance of different backbone networks has been improved.

As can be seen from Figure 10, when the training data is inconsistent with the test data, the average improvement of the model with PIM in the five training domains A, B, C, D, and A/B/C to the test domain is 1.9%, –0.71%, 2.1%, 8.4%, and 2.0% respectively. Therefore, PIM can improve the fault identification performance of the network under the variable parameters of the motor, and make the network have certain characteristics of resistance to variable parameters.

Comparing the results of the network with training domains A/B/C, A, B and C with the test domain D, it can be found that when the network parameters are closer, the stronger the ability of the network to resist changing parameters, the difference between C and D parameters is the smallest, and the similarity of feature space is the largest. When PIM is not used, the test accuracy of network models with training domains C and A/B/C is nearly 14% different than that of D domain. It shows that using more data to enrich the model feature domain is helpful to improve the model fault recognition performance under variable parameters. After adding PIM to enrich the feature domain, the accuracy of both D domain is improved respectively. It is not difficult to find that adding PIM to the model is helpful to enrich the feature domain, and the performance improvement is greater for the model with less feature domain than the model with larger feature domain

5 Conclusions

In this paper, two problems faced by motor fault diagnosis based on deep learning are studied, namely, the decline of fault recognition accuracy caused by motor parameter changes and the problem of small samples, and a motor fault diagnosis method based on deep transfer learning is proposed. Moreover, this paper introduces the causes, functions and conception process of this method in detail, and briefly introduces how to select motor fault characteristic signals. Then, through four sets of experiments, this paper gradually analyses the performance, effectiveness and advancement of the network in the face of variable parameter problems and small sample problems. From the experimental results, it can be seen that the motor fault diagnosis method based on deep transfer learning proposed in this paper is feasible and effective in CWRU public dataset, and can solve the problem of decreasing accuracy of neural network fault recognition caused by motor variable parameters, insufficient number of target samples, unlabeled target samples and other small sample problems to some extent.

At the same time, this paper provides a large number of engineering measured data for the problem of insufficient samples faced by complex machinery such as motors, which lays a good foundation for follow-up research. In the follow-up, it is necessary to carry out experimental tests for other types of motor faults that are not involved in the experiment in this paper. In addition, it is necessary to train the PIM and the basic network model with generative models such as generative adversarial networks and auto-encoders to improve the fault diagnosis stability of the network under variable parameters.

This paper uses CWRU and MFPT datasets to carry out experiments, focusing on the specific motor fault types. It is necessary to discuss how to extend the method to other fault types or datasets not involved in this study, which will help to promote the method.

Declarations

This research was supported by the Scientific Research and Innovation Team Construction Project of Hunan Railway Professional Technology College (Grant No. KYTD202401) and Hunan Provincial Natural Science Foundation of China (Grant No. 2025JJ80366) and the Scientific Research Project of the Hunan Provincial Department of Education (Grant No. 24C1065).

All authors declare that they have no conflicts of interest.

References

Almounajjed, A., Sahoo, A.K., Kumar, M.K. and Assaf, T. (2022) 'Fault diagnosis and investigation techniques for induction motor', *International Journal of Ambient Energy*, Vol. 43, No. 1, pp.6341–6361.

AlShorman, O., Irfan, M., Saad, N., Zhen, D., Haider, N., Glowacz, A. and AlShorman, A. (2020) 'A review of artificial intelligence methods for condition monitoring and fault diagnosis of rolling element bearings for induction motor', *Shock and Vibration*, Vol. 1, No. 1, pp.8843759–8843771.

Cheng, J.H., Lu, C.L., Zhang, G., Wang, B. and Fang, J. (2021) 'Design of motor intelligent monitoring and fault diagnosis system based on LoRa', *IEEE Transactions on Applied Superconductivity*, Vol. 31, No. 8, pp.1–4.

Gundewar, S.K. and Kane, P.V. (2021) 'Condition monitoring and fault diagnosis of induction motor', *Journal of Vibration Engineering & Technologies*, Vol. 9, No. 7, pp.643–674.

Lang, W., Hu, Y., Gong, C., Zhang, X., Xu, H. and Deng, J. (2021) 'Artificial intelligence-based technique for fault detection and diagnosis of EV motors: a review', *IEEE Transactions on Transportation Electrification*, Vol. 8, No. 1, pp.384–406.

Liang, Y., Li, B. and Jiao, B. (2021) 'A deep learning method for motor fault diagnosis based on a capsule network with gate-structure dilated convolutions', *Neural Computing and Applications*, Vol. 33, No. 2, pp.1401–1418.

Lin, S.L. (2021a) 'Application combining VMD and ResNet101 in intelligent diagnosis of motor faults', *Sensors*, Vol. 21, No. 18, pp.6065–6077.

Lin, S.L. (2021b) 'Intelligent fault diagnosis and forecast of time-varying bearing based on deep learning VMD-DenseNet', *Sensors*, Vol. 21, No. 22, pp.7467–7479.

Long, Z., Zhang, X., He, M., Huang, S., Qin, G., Song, D. and Shao, H. (2021a) 'Motor fault diagnosis based on scale invariant image features', *IEEE Transactions on Industrial Informatics*, Vol. 18, No. 3, pp.1605–1617.

Long, Z., Zhang, X., Song, D., Tang, Y., Huang, S. and Liang, W. (2021b) 'Motor fault diagnosis using image visual information and bag of words model', *IEEE Sensors Journal*, Vol. 21, No. 19, pp.21798–21807.

Nath, A.G., Udmale, S.S. and Singh, S.K. (2021) 'Role of artificial intelligence in rotor fault diagnosis: a comprehensive review', *Artificial Intelligence Review*, Vol. 54, No. 4, pp.2609–2668.

Niu, G., Dong, X. and Chen, Y. (2023) 'Motor fault diagnostics based on current signatures: a review', *IEEE Transactions on Instrumentation and Measurement*, Vol. 726, No. 1, pp.1–19.

Saha, D.K., Hoque, M.E. and Badihi, H. (2022) 'Development of intelligent fault diagnosis technique of rotary machine element bearing: a machine learning approach', *Sensors*, Vol. 22, No. 3, pp.1073–1086.

Shao, H., **a, M., Han, G., Zhang, Y. and Wan, J. (2020) 'Intelligent fault diagnosis of rotor-bearing system under varying working conditions with modified transfer convolutional neural network and thermal images', *IEEE Transactions on Industrial Informatics*, Vol. 17, No. 5, pp.3488–3496.

Shen, J., Li, S., Jia, F., Zuo, H. and Ma, J. (2020) 'A deep multi-label learning framework for the intelligent fault diagnosis of machines', *IEEE Access*, Vol. 8, No. 3, pp.113557–113566.

Sun, M., Wang, H., Liu, P., Long, Z., Yang, J. and Huang, S. (2022) 'A novel data-driven mechanical fault diagnosis method for induction motors using stator current signals', *IEEE Transactions on Transportation Electrification*, Vol. 9, No. 1, pp.347–358.

Tang, S., Yuan, S. and Zhu, Y. (2020) 'Convolutional neural network in intelligent fault diagnosis toward rotatory machinery', *IEEE Access*, Vol. 8, No. 2, pp.86510–86519.

Wang, C. and Xu, Z. (2021) 'An intelligent fault diagnosis model based on deep neural network for few-shot fault diagnosis', *Neurocomputing*, Vol. 456, No. 1, pp.550–562.

Wang, Y., Yan, J., Sun, Q., Jiang, Q. and Zhou, Y. (2020) 'Bearing intelligent fault diagnosis in the industrial internet of things context: a lightweight convolutional neural network', *IEEE Access*, Vol. 8, No. 4, pp.87329–87340.

Xue, H., Wu, M., Zhang, Z. and Wang, H. (2022) 'Intelligent diagnosis of mechanical faults of in-wheel motor based on improved artificial hydrocarbon networks', *ISA Transactions*, Vol. 1203, No. 1, pp.360–371.

Yin, J. and Cen, G. (2022) 'Intelligent motor bearing fault diagnosis using channel attention-based CNN', *World Electric Vehicle Journal*, Vol. 13, No. 11, pp.208–220.

Zhang, T., Chen, J., Li, F., Zhang, K., Lv, H., He, S. and Xu, E. (2022) 'Intelligent fault diagnosis of machines with small & imbalanced data: a state-of-the-art review and possible extensions', *ISA Transactions*, Vol. 119, No. 3, pp.152–171.